Transient Confinement of a Glycosylphosphatidylinositol-Anchored Protein in the Plasma Membrane†

Erin D. Sheets,‡ Greta M. Lee,§,|| Rudolf Simson,§,⊥ and Ken Jacobson*,§,#

Departments of Chemistry and Cell Biology & Anatomy, and Lineberger Comprehensive Cancer Center, University of North Carolina, Chapel Hill, North Carolina 27599

Received May 9, 1997; Revised Manuscript Received August 19, 1997⊗

ABSTRACT: Glycosylphosphatidylinositol (GPI)-anchored proteins participate in many cell surface functions; however, the molecular associations of these lipid-linked proteins within the plasma membrane are not well understood. Recent biochemical analyses of detergent insoluble membrane fractions have suggested that GPI-anchored proteins may be associated with glycosphingolipid (GSL)-enriched domains that also contain cholesterol and signaling molecules such as Src family kinases and, in some cases, caveolae. The movements of two components of the putative GSL-enriched domains, Thy-1, a GPI-anchored protein, and GM1, a GSL, were followed with single particle tracking on C3H 10T1/2 cell surfaces and categorized into four modes of lateral transport, fast diffusion, slow anomalous diffusion, diffusion confined to 325−370 nm diameter regions, and a fraction of molecules that was essentially stationary on the 6.6 s time scale. Longer observations (60 s) showed that Thy-1 and GM1 are transiently confined for 7−9 s to regions averaging 260−330 nm in diameter. Approximately 35−37% of both Thy-1 and GM1 undergo confined diffusion, whereas only 16% of fluorescein phosphatidylethanolamine, a phospholipid analog which is not expected to be found in the GSL domains, experience confined diffusion to regions averaging ∼230 nm in diameter. Further, when glycosphingolipid expression was reduced ∼40% with the glucosylceramide synthase inhibitor, D-*threo*-1-phenyl-2-decanoylamino-3-morpholino-1-propanol, the percentage of trajectories exhibiting confinement and the size of the confining domain for Thy-1 were reduced ∼1.5-fold. In contrast, extraction of cells with Triton X-100 leaves the fraction of molecules confined and the domain sizes of Thy-1 and GM1 unchanged. Our results are consistent with the preferential association of GPI-anchored proteins with glycosphingolipid-enriched domains and suggest that the confining domains may be the *in vivo* equivalent of the detergent insoluble membrane fractions.

Understanding the molecular associations of glycosylphosphatidylinositol (GPI[1])-anchored proteins within the plasma membrane has been the subject of much recent work. These lipid-anchored proteins have been postulated to be associated with glycosphingolipid (GSL) domains that are thought to be enriched with Src-related tyrosine kinases, heterotrimeric G proteins, cholesterol, and for some cells types, caveolin (for review, see refs 1−3). The glycosphingolipid domains and their molecular components have been characterized in biochemical analyses of both detergent insoluble cell lysates that have been isolated by sucrose density gradient centrifugation (*4*−*8*) and membrane fractions isolated using silica particles (*9*). The presence of signaling molecules in the insoluble fractions has led to the hypothesis that these glycosphingolipid domains may localize GPI-anchored proteins to regions specialized for cellular signaling, and may in fact explain the mechanisms by which GPI-anchored proteins can activate cells (*10*−*13*). With few exceptions (*14*, *15*), however, the putative glycosphingolipid domains have not been directly observed *in vivo*.

Previous work which investigated the lateral mobilities of GPI-anchored proteins using fluorescence recovery after photobleaching (FRAP) showed that some GPI-anchored proteins, such as Thy-1, Qa-2, and neural cell adhesion molecules (*16*−*18*), exhibited lateral diffusion coefficients (D) similar to those of lipids (10^{-9}−10^{-8} cm^2/s). However, unlike lipids which, in most cases, are 80−100% mobile in the plasma membrane, a significant fraction (∼50%) of the lipid-linked proteins were unable to undergo lateral diffusion (*16*−*18*). These results and results from other biophysical measurements of membrane-spanning proteins, whose movements are also highly restricted, have suggested considerable revision of our understanding of the plasma membrane structure, as described in several recent reviews (*19*−*23*).

In this work, we used single particle tracking (SPT) to gain insight into the mechanisms that cause the substantial immobile fractions observed in the FRAP measurements for

† Supported by National Institutes of Health Grant GM-41402.

* Address correspondence to: Department of Cell Biology & Anatomy, University of North Carolina, Chapel Hill, NC 27599-7090; 919 966-5703 (phone); 919 966-1856 (fax); frap@med.unc.edu (e-mail).

‡ Department of Chemistry. Present address: Department of Chemistry, Cornell University, Ithaca, NY 14853-1301.

§ Department of Cell Biology & Anatomy.

|| Present address: Department of Orthopedics, Thurston Arthritis Research Center, University of North Carolina, Chapel Hill, NC 27599.

⊥ Present address: Technical University of Munich, Institute for Biophysics E22, 85748 Garching, Germany.

Lineberger Comprehensive Cancer Center.

⊗ Abstract published in *Advance ACS Abstracts,* October 1, 1997.

[1] Abbreviations: BME, Basal Medium Eagle with Earle's salts and L-glutamine; *D*, lateral diffusion coefficient; FBS, fetal bovine serum; fl-PE, *N*-(5-fluoresceinthiocarbamoyl)-1,2-dihexadecanoyl-*sn*-glycero-3-phosphoethanolamine; FRAP, fluorescence recovery after photobleaching; GPI, glycosylphosphatidylinositol; GSL, glycosphingolipid; HH, Hams F12 medium/25 mM HEPES; HHS, Hams F12 medium/25 mM HEPES/10% FBS; LDL, low density lipoprotein; NANA, *N*-acetylneuraminic acid; PDMP, D-*threo*-1-phenyl-2-decanoylamino-3-morpholino-1-propanol·HCl; PL, phospholipid; SPT, single particle tracking; TX-100, Triton X-100.

S0006-2960(97)01093-3 CCC: $14.00

GPI-anchored proteins. The movements of individual (or a few) molecules on the cell surface that have been specifically labeled with colloidal gold or fluorescent particles can be measured with nanometer precision by SPT (*24*−*29*). In the work described here, video-enhanced brightfield microscopy was used to detect 40 nm diameter ligand-coated colloidal gold particles that were bound to specific molecules and detected as dark spots where the light had been scattered by the gold probes. The movements of the membrane components were recorded for a defined period of time, and the centroids of each particle determined in every image of a recorded sequence. The connected centroids are the trajectories that individual molecules followed during the observation period.

In the present work, we followed the movements of Thy-1, the smallest member of the immunoglobulin superfamily, on the surfaces of C3H 10T1/2 fibroblasts. We find that 37% of the Thy-1 molecules experience transiently confined diffusion for an average of 7 s to small domains that are ∼300 nm in diameter. We also investigated the lateral movements of two types of lipids, GM1, a glycosphingolipid and putative component of GSL-enriched domains, and fluorescein phosphatidylethanolamine, a phospholipid analog. We find that GM1 exhibits similar confined behavior as Thy-1, whereas the phospholipid analog undergoes significantly less confined diffusion. We also observed a ∼1.5-fold decrease in the fraction of confined Thy-1 and the size of the confining domains on the surfaces of glycosphingolipid-depleted fibroblasts. However, little change was observed for either the fractions of Thy-1 and GM1 experiencing confined diffusion or the sizes of the confinement regions on cell membranes that had been extracted with Triton X-100. These results are consistent with the idea of preferential association of GPI-anchored proteins with glycosphingolipid-enriched domains.

EXPERIMENTAL PROCEDURES

Gold Conjugation. *anti*-Thy-1 (T24/31.7; I. Trowbridge, Salk Institute, La Jolla, CA) and *anti*-fluorescein (2-3-6; E. Voss, University of Illinois at Urbana-Champaign) were conjugated at pH 8.9 to 40 nm diameter colloidal gold (Ted Pella, Redding, CA), and cholera toxin B was conjugated at pH 6.9 to 40 nm colloidal gold, as described previously (*30*).

Cells. C3H 10T1/2 fibroblasts (American Type Culture Collection, Rockville, MD) were maintained in Basal Medium Eagle with Earle's salts and L-glutamine (BME) that had been supplemented with 10% fetal bovine serum (FBS), 100 units/mL penicillin and 100 μg/mL streptomycin. Two to four days before a SPT experiment, fibroblasts were plated onto sterile 22 mm × 22 mm coverslips (#1, glass) that had been placed into 35 mm petri dishes, at an appropriate cell density that yielded single cells for SPT measurements.

Single Particle Tracking. Immediately before a SPT experiment, an aliquot of gold-conjugated protein was washed twice with Hams F12 medium that had been supplemented with 25 mM HEPES and 10% FBS (HHS) and pelleted in a microcentrifuge (10 000 rpm, 10 min, 4 °C); after the second wash, the gold pellet was resuspended in a volume of HHS that would yield an adequate density of gold on the cell surfaces (typically, 20−60 particles/cell). Cells were washed twice for 2 min with warm (∼37 °C) Hams F12 and 25 mM HEPES (HH) medium and placed onto a 100 μL droplet of the gold suspension that had been applied to the center of a 3 in. × 1 in. glass slide and incubated for 15 min in a humidified environment. Cells were washed twice with 100 μL HHS and sealed with vaseline:lanolin:dental wax, 1:1:2, w/w.

A Hamamatsu newvicon camera with a 4× magnifier was used to record images of colloidal gold bound to cells under brightfield optics on a Zeiss Axiovert-10 with a Zeiss Plan-Neofluar 100× oil-immersion objective (NA 1.3) and oil-immersion achromatic/aplanatic condenser (NA 1.4), as described previously (*27*, *30*). Video sequences were recorded to an optical memory disk for 6.6 s (200 frames at video rate [30 frames/s]) and for 60 s (200 frames at 3 frames/s). Particle centroids were calculated using the cross-correlation method of Gelles *et al.* (*31*) as implemented in Image-1 software (Universal Imaging, West Chester, PA). Trajectories from single particle tracking recordings that were ≥3/4 complete were analyzed. All SPT experiments were done at 37 °C, which was maintained with an air curtain incubator.

For the SPT experiments of the phospholipid analog, *N*-(5-fluoresceinthiocarbamoyl)-1,2-dihexadecanoyl-*sn*-glycero-3-phosphoethanolamine (fl-PE; Molecular Probes, Eugene, OR), cells were washed 3 times with HH. fl-PE in ethanol (40 μL of 1 mg/mL) was diluted to 2 mL with HH, vortexed vigorously, and immediately added to the petri dish. After incubating at 37 °C for 10 min in the dark, the cells were quickly rinsed 3 times with HH and prepared as described above.

To demonstrate the binding specificity of the gold-conjugated protein, we coincubated, on the day of each experiment, some SPT samples with 1 μM excess antibody or cholera toxin B or 100 μM sodium fluorescein in the presence of the gold probe at experimental concentrations. Significantly reduced gold binding (0−5 bound gold particles/cell) was consistently observed with the negative controls, as compared to the positive samples (20−60 bound gold particles/cell). For the fl-PE SPT experiments, we also examined *anti*-fluorescein/gold binding to cell surfaces when fl-PE had not been incorporated into the plasma membrane; these negative control samples also yielded <5 bound gold particles/cell.

Paucivalent Gold SPT Experiments. To determine the effects of gold/protein valency or activity, we mixed *anti*-Thy-1 with goat IgG at the following *anti*-Thy-1:goat IgG molar ratios: 1:29, 1:19, 1:9, 1:4, and 1:1.5. The 1:1.5 molar ratio gold probe was the only *anti*-Thy-1:goat IgG mixture that yielded gold binding at levels greater than the negative controls, and this probe was used for SPT experiments.

Lipid Depletion Experiments. Four days before some SPT experiments, cells were plated onto coverslips and allowed to adhere for 6−7 h. Spent medium was removed and replaced with fresh medium (BME/10% FBS/100 units/mL penicillin/100 μg/mL streptomycin) that contained the presence or absence of lipid depleting reagents. For glycosphingolipid depletion, 10 μM D-*threo*-1-phenyl-2-decanoylamino-3-morpholino-1-propanol·HCl (PDMP; Matreya, Pleasant Gap, PA), an inhibitor of glucosylceramide synthase, was used (*32*−*34*). Cholesterol depletion was accomplished by supplementing media with 10% LDL-depleted FBS, 200 μM mevalonate, and 25 μM mevastatin (*35*, *36*).

Lipid Assays. During the morning of the glycosphingolipid-depleted SPT experiments, phospholipids and glycosphingolipids were isolated from 75 cm^2 flasks containing $(1-2) \times 10^6$ control or PDMP-treated cells (*37*) to obtain a measure of the extent of GSL depletion. Briefly, lipids were extracted from the cell pellet with $CHCl_3$:MeOH:H_2O (1:2:0.75, v/v). Phospholipids were separated from glycolipids after adjusting the volumetric ratio of $CHCl_3$:MeOH:H_2O to 4:8:5.6 and reextracting. The upper phases (composed of methanol and water) were transferred to new screw top tubes, and the lower phases were reextracted with 10 mM KCl:MeOH to bring the final volumetric ratio of solvents to $CHCl_3$:MeOH:10 mM KCl ratio to 4:8:5.6. The lower phases (containing phospholipids) were dried under nitrogen and stored at −20 °C under nitrogen. The upper phases (containing glycolipids) were dialyzed (1000 molecular weight cutoff membrane) against H_2O at 4 °C. After dialysis, the glycolipid suspensions were dried and stored under nitrogen at −20 °C. The paired control and treated samples were manipulated simultaneously to control for handling.

The quantity of phospholipids was assayed by the inorganic phosphorus method of Bartlett (*38*−*40*). Briefly, phospholipids were resuspended in 1 mL of H_2O immediately before the assay with vigorous vortexing and sonication and combusted with 18 M H_2SO_4 and 30% H_2O_2. To each tube were added 650 μL of H_2O, 200 μL of 5% (w/v) ammonium molybdate (freshly prepared), and 50 μL of Fiske−Subbarow reagent [prepared as described (*38*)]. The samples were heated in a boiling H_2O bath for 7 min, and absorbances were read at 830 nm. The phosphate standards were fit to a line by the least-squares method and phospholipid quantities estimated.

Glycosphingolipid quantities were estimated by assaying the *N*-acetylneuraminic acid (NANA) content of the glycolipid fraction (*41*, *42*). Briefly, glycolipid samples were resuspended in 0.25 mL H_2O by vortexing and sonication. Standards (0.5 mL) containing 0−50 μg of NANA were prepared in 13 mm × 100 mm screw top tubes. (The glycolipid sample volumes and all volumes of the following reagents were decreased by half to increase the sensitivity of the assay; the volumes given were those used for the standards.) To each tube was added 100 μL of 0.04 M periodic acid. After mixing, the standards were placed on ice for 20 min, whereas the lipid samples were incubated at 37 °C for 1 h. The tubes were chilled on ice briefly, and 1.2 mL of freshly prepared resorcinol reagent [1.44 mL of 6% (w/v) resorcinol/4.32 mL of H_2O/8.64 mL of 28% HCl/36 μL of 0.1 M $CuSO_4$] was added to each tube. The samples were mixed, incubated on ice for 5 min, and heated in a boiling H_2O bath for 15 min. After cooling briefly, 1.25 mL of 2-methyl-2-propanol was mixed with each sample to obtain one phase. The tubes were incubated at 37 °C for 15 min to achieve color stabilization, and absorbances were read at 620 nm. The NANA standards were fit to a line by the least-squares method, and NANA content of the glycosphingolipid samples was estimated.

The extent of glycosphingolipid depletion was estimated as follows. The NANA/PL molar ratio was calculated. The ratio of the depleted NANA/PL to control NANA/PL was determined for each pair of samples, and the mean and SEM were calculated.

All glassware (except for the tissue grinder) was cleaned in ethanolic KOH. Unless noted otherwise, all manipulations were carried out at room temperature.

Triton X-100 Extraction Experiments. Immediately before a SPT experiment, petri dishes containing cells that had been plated onto coverslips (see above) were placed on ice and quickly washed 3 times with ice cold HHS. The coverslips were then incubated with HHS ± [0.1% Triton X-100 (TX-100)/0.01 units/mL aprotinin/0.1 mM phenylmethanesulfonyl fluoride] for 30 min at 4 °C on ice. The coverslips were quickly rinsed 3 times with cold HHS to remove the detergent, and then they were prepared for SPT experiments as described above.

Probability Profile Analysis of 60 s Trajectories. We used the probability profile analysis described by Simson *et al.* (*43*) to identify periods of transient confinement in trajectories from the 60 s observations. Briefly, the probability Ψ that a randomly diffusing particle will remain in a particular region of radius R for a window of time t is calculated following Saxton (*43*, *44*), where $\log \Psi = 0.2048 - 2.5117(Dt/R^2)$. To accentuate nonrandom behavior graphically, the probability is then converted to a probability level, L, where $L = -\log \Psi - 1$. Higher L values indicate a higher probability of nonrandom behavior. Parameters such as the threshold, the size and overlap of the windows, and the minimum duration were optimized by simulating 1100 random walks, and conditions were found in which only 1.5% of the simulated random tracks showed confined mobility (*43*).

RESULTS

Thy-1 Exhibits Four Modes of Transport on a 6.6 s Time Scale. We developed a method for categorizing the lateral mobility of membrane components on the surfaces of cells. This method, which is based upon the work of Saxton (*44*) and is described more fully elsewhere (*45*, R. Simson, S. E. Moore, P. Doherty, F. S. Walsh, and K. A. Jacobson, unpublished results), is dependent upon classifying SPT trajectories from 6.6 s observations into one of four modes of lateral transport, fast diffusion, slow diffusion, confined diffusion, and a "stationary" fraction of molecules whose movements (70−100 nm) during our 6.6 s observation period are slightly greater than the limits of our spatial resolution (∼30 nm). In addition to the initial lateral diffusion coefficients (D), the parameters we use to classify the tracks are based upon the ellipses of gyration that characterize each trajectory (*44*). The radius of gyration, R_g^2, is used as a measure of the area covered by the trajectory and is defined as $R_g^2 = R_1^2 + R_2^2$, where R_1 and R_2 are the respective major and minor semiaxes of the ellipse. The asymmetry of the track is given by a_2, which is defined as $a_2 = R_2^2/R_1^2$. The shapes of the associated mean squared displacement plots are also critical for classifying tracks to specific modes of transport.

Representative trajectories for each mode of transport are shown in Figure 1, and Table 1 shows the mean values of D, R_g^2, and a_2 obtained from the trajectory classification of Thy-1. We assign each parameter of a particular trajectory to a transport mode and categorize it based upon the general trend in the individual parameters. For example, the tracks for the rapidly and slowly diffusing classes tend to be more asymmetric ($a_2 < 0.5$) than the confined diffusion and stationary classes (a_2 on average is $\gtrsim 0.5$). R_g^2 (which is

Table 1: Classification of Thy-1 Movements from a 6.6 s Time Scale into Four Modes of Transport[a]

		D ($\times 10^{-10}$ cm^2/s)	R_g^2 (μm^2)	a_2
Thy-1, $n = 295$	fast	8.1 ± 0.7	0.34 ± 0.04	0.23 ± 0.02
	slow	0.35 ± 0.05	0.013 ± 0.002	0.28 ± 0.02
	confined	0.98 ± 0.18	0.013 ± 0.003	0.48 ± 0.02
	stationary	0.060 ± 0.014	0.0011 ± 0.0001	0.50 ± 0.04
Thy-1 (GSL depleted), $n = 90$	fast	4.7 ± 0.9	0.19 ± 0.04	0.26 ± 0.04
	slow	0.44 ± 0.07	0.014 ± 0.003	0.25 ± 0.03
	confined	0.54 ± 0.10	0.0065 ± 0.0010	0.44 ± 0.04
	stationary	0.11 ± 0.04	0.0016 ± 0.0003	0.46 ± 0.07
GM1, $n = 127$	fast	6.9 ± 0.6	0.26 ± 0.03	0.27 ± 0.03
	slow	0.80 ± 0.16	0.021 ± 0.003	0.33 ± 0.04
	confined	1.4 ± 0.3	0.017 ± 0.004	0.43 ± 0.03
	stationary	0.074 ± 0.021	0.0014 ± 0.0003	0.53 ± 0.04
fl-PE, $n = 106$	fast	5.6 ± 0.6	0.21 ± 0.04	0.33 ± 0.03
	slow	0.38 ± 0.06	0.016 ± 0.003	0.31 ± 0.03
	confined	0.55 ± 0.16	0.0066 ± 0.0021	0.48 ± 0.04
	stationary	0.15 ± 0.03	0.0017 ± 0.0002	0.56 ± 0.05

[a] Tracks are categorized according to the initial lateral diffusion coefficients (D) (estimated by fitting the initial slope of the associated mean squared displacement plots, where the slope is $4D$), the radii of gyration (R_g^2), asymmetry (a_2), and the shapes of the associated mean squared displacement plots (see Figure 3A), as described in the text. All values are reported as the mean ± SEM. n is the number of trajectories analyzed.

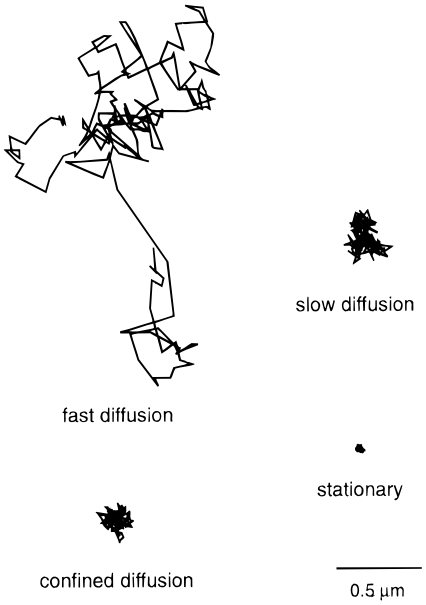

FIGURE 1: These four trajectories of Thy-1 movements in C3H plasma membranes are representative of the four modes of transport into which we classify tracks from 6.6 s observations.

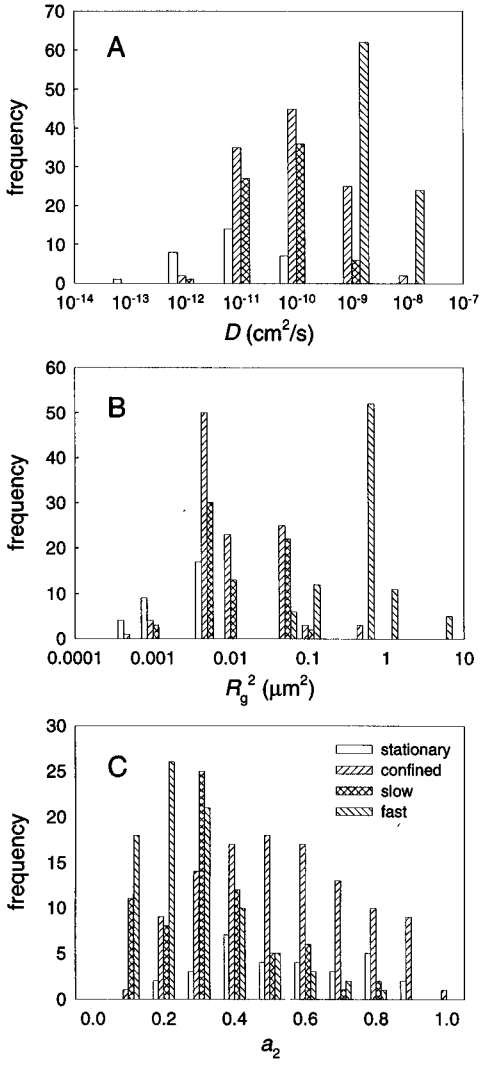

FIGURE 2: Distributions of the 6.6 s classification parameters for Thy-1 are shown for the initial lateral diffusion coefficients (A), R_g^2 (B), and a_2 (C).

dependent upon D) differentiates between the fast ($R_g^2 \geq 0.07$ μm^2) and slow and confined classes ($R_g^2 < 0.07$ μm^2), and R_g^2 for the stationary class is <0.002 μm^2. The distributions of the parameters after classification of the 6.6 s Thy-1 trajectories are shown in Figure 2. The primary criterion used to distinguish slow diffusion from confined diffusion is the shape of the mean squared displacement plot associated with each trajectory, as can be readily seen by comparing the shape of the plot of slow diffusion (dashed line in Figure 3A) with that of confined diffusion (dotted line in Figure 3A). When the time in a confining region is on the same order of the experimental time scale, the mean squared displacement ($<r^2>$) versus time plots of individual trajectories for the confined class approaches a limiting value (which is the square of the radius, $<r_o^2>$, of the confining region) (*24*), whereas $<r^2>$ for slow diffusion has an approximately linear relationship with respect to time τ, as expected for a random walk (see Figure 3A). The radius of the confining region can be calculated as $r_o = (2\ R_g^2)^{1/2}$ (*44*) and is shown in Table 2. When the size of the domain is extrapolated from the mean squared displacement plots for confined diffusion, there is good agreement with the more exact values calculated from R_g^2, which are derived from the individual trajectories (data not shown).

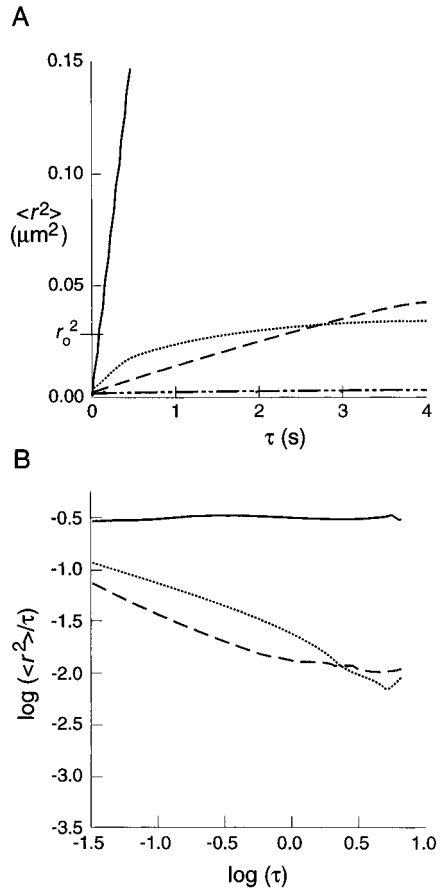

FIGURE 3: (A) The averaged mean squared displacements ($<r^2>$) for each category of Thy-1 behavior described in Table 1 are plotted as a function of time interval τ. Mean squared displacement plots for confined diffusion (dot) approach an asymptotic limit $<r_o^2>$, the squared radius of the confining region. Other plots are fast diffusion (solid line), slow diffusion (dash), and stationary (dash dot dot). (B) Anomalous diffusion can be detected from the initial slopes when log ($<r^2>/\tau$) is plotted as a function of log τ for the averaged mean squared displacement plots for each mode of transport (*48*). Anomalous diffusion is determined from the slope, $\alpha - 1$, where α is the anomalous diffusion exponent. For normal random diffusion, $\alpha \approx 1$ (*48*). The shapes of these two graphs are representative for all SPT experiments reported.

Table 2: Distributions of the 6.6 s Trajectory Classification

molecule	fast	slow	confined	stationary	*n*
Thy-1	29%	24%	37% 322 ± 38 nm[a]	10%	295
Thy-1 (GSL depleted)	28%	34%	28% 228 ± 18 nm	10%	90
GM1	33%	20%	35% 369 ± 44 nm	13%	127
fl-PE	42%	33%	16% 230 ± 37 nm	9%	106

[a] The diameter of the confining region was calculated from $r_o = (2R_g^2)^{1/2}$ (*44*) and is reported as mean ± SEM.

To test further our ability to distinguish between slow and confined diffusion by this classification scheme, we simulated 200 random walks that had been generated with $D = 6.9 \times 10^{-11}$ cm^2/s (the approximate D for confined and slow diffusion, see below and Table 1) and an experimental time scale of 6.6 s. We found that 9.5% of the pure random walks were misidentified as confined diffusion.

The distribution of the modes of lateral transport and the respective diffusion coefficients for Thy-1 are shown in Tables 1 and 2. The lateral diffusion coefficient for the 29% of Thy-1 undergoing fast diffusion [$(8.1 \pm 0.7) \times 10^{-10}$ cm^2/s] is within a factor of 5 of the D obtained by FRAP [$\sim 4 \times 10^{-9}$ cm^2/s (*16*)]; diffusion coefficients obtained by SPT are generally 2−6-fold lower than those obtained by FRAP (*24*). Thy-1 (24%) underwent slow diffusion [$(0.35 \pm 0.05) \times 10^{-10}$ cm^2/s]. The slow diffusion may be attributed to much larger micrometer-sized domains in the plasma membrane, the boundaries of which would not be detected with SPT observations of this length. Thy-1 (37%) experienced confined diffusion to regions that were ∼325 nm in diameter.

Table 3: Domain Sizes and Confinement Times Determined by the Probability Profile Analyses of 60 s Tracks[a]

molecule	domain diameter (nm)	confinement time (s)	*n*
Thy-1	260± 21	6.9 ± 0.8	29
Thy-1 (GSL depleted)	165± 17	6.3 ± 0.9	11
GM1	332± 62	8.6 ± 1.8	19
fl-PE	222± 14	5.6 ± 0.5	19

[a] All values are reported as the mean ± SEM. *n* is the number of tracks exhibiting confined diffusion.

The Confinement of Thy-1 Is Transient. When we observed the movements of Thy-1 (or other membrane components) for longer periods (≥1 min), we saw no particles remaining stationary for the entire duration of observation, suggesting that the plasma membrane can transiently confine molecules depending upon local molecular interactions and micrometer- and submicrometer-sized lateral inhomogeneities in the membrane. To identify periods of transient confinement, we developed a method based upon the probability of a random diffusant remaining in a defined region for a given period of time (see Figure 4) (*43*). This fundamentally different method of analysis of the 60 s data also demonstrates that Thy-1 molecules are confined to domains 260 nm in diameter, for ∼7 s (Table 3 and Figure 5), consistent with the results from the 6.6 s data (Table 2). The tracks that exhibited transient confinement contained 1−4 periods of confinement.

Reducing Valency of the Gold Probe Does Not Affect Classification. To determine whether the observed transient confinement of Thy-1 was an artifact of the multivalent nature of the colloidal gold probe, we mixed *anti*-Thy-1 with goat IgG at the following molar ratios: 1:29, 1:19, 1:9, 1:4, and 1:1.5. Only gold conjugated with the 1:1.5 antibody mixture yielded gold binding to cell surfaces at levels above background. We then used the 1:1.5 mixture/gold conjugate (termed here, paucivalent) and compared the results of our classification to those obtained with gold conjugated only to *anti*-Thy-1 (multivalent for this experimental comparison). As shown in Table 4, we find good agreement between the percentages of confined diffusion exhibited by paucivalent and multivalent gold particles as well as the size of the confining domain (325−400 nm in diameter). We also see good agreement with the size of the confining domain (260−280 nm) and confinement time (7−10 s) when we apply the probability profile analysis to the 60 s tracks. These results indicate that the valency of the gold probe does not have a major effect on either our classification scheme or the detection of transient confinement.

When Thy-1 and other membrane proteins form higher order aggregates by binding to multivalent probes, they often undergo capping which is indicative of the aggregates being

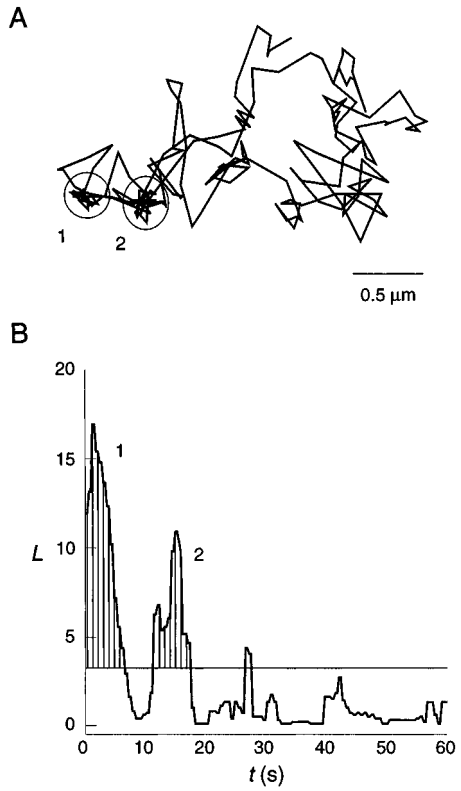

FIGURE 4: Regions of transient confinement which may be obscured by other parts of the trajectory are located by identifying sections of the trajectory (A) that are undergoing nonrandom diffusion with a probability profile; the peaks denote periods where molecules remain in a defined region for much longer times than expected for random diffusant (B). The probability level L is calculated as described (*43*) and is plotted as a function of the time t. The horizontal threshold in Figure 4B corresponds to $L = 3.15$, a likelihood of <0.007% of being of random origin (*43*). Note that the third peak is not considered to be a period of confinement because the peak does not exceed the minimum duration necessary to qualify as a confinement domain.

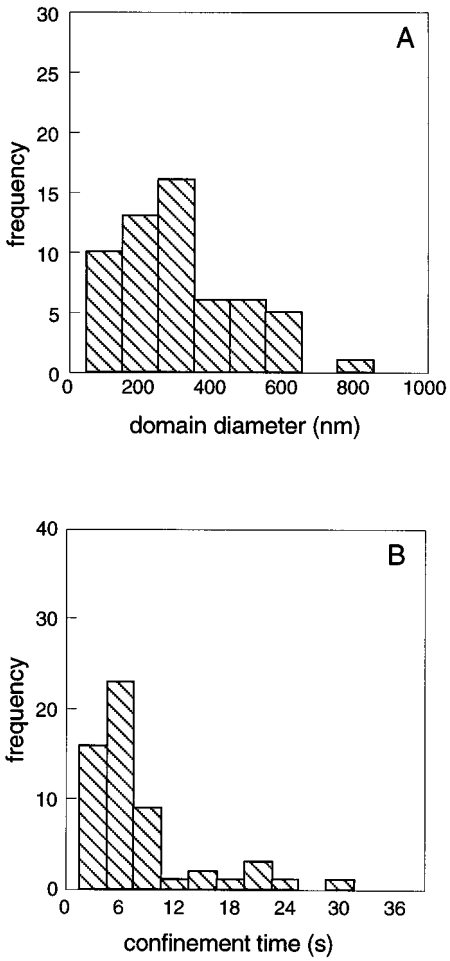

FIGURE 5: The probability profile analysis was used to identify periods of transient confinement in Thy-1 trajectories from 60 s observation periods. The distributions of (A) the diameter of the confining domain and (B) the confinement time for individual confinement periods are shown. We observed 1−4 periods of transient confinement within individual trajectories.

raked by cortical cytoskeletal flow (*46*). However, we observe no trajectories exhibiting directed motion, which occurs when membrane proteins are bound to the cytoskeleton (*28*, *47*). Thus, the absence of directed motion in the work reported here is further evidence that the valency of the gold probe is not sufficient to cause a serious perturbation.

Thy-1 Exhibits Anomalous Diffusion. Anomalous diffusion occurs when the diffusion of a molecule is hindered by moving through a dense field of obstacles (*48*−*50*). Simple random diffusion has a linear dependence of the mean squared displacement $<r^2>$ on time τ (see Figure 3A); however, for anomalous diffusion, $<r^2> \propto \tau^{\alpha}$, where α is the anomalous diffusion exponent, and is easily recognized by a negative slope of $(\alpha - 1)$ when $\log(<r^2>/\tau)$ is plotted as a function of $\log \tau$ (Figure 3B) (*48*, *50*). A more qualitative way of thinking about anomalous diffusion is as follows. At very short periods of time, a diffusing molecule does not encounter enough obstacles to impede lateral diffusion significantly, so diffusion is approximately normal. At longer times, however, the molecule can encounter many more obstacles that will obstruct its diffusion, leading to anomalous diffusion. If after some time the molecule diffuses away from the obstacles and enters a region with fewer barriers, such as the lipid continuum, diffusion again becomes normal.

Although the fast diffusion class exhibits normal Brownian motion, we observe that slow diffusion and confined diffusion display anomalous diffusion, as shown in Figure 3B and Table 5. The slow diffusion and confined diffusion categories experience anomalous diffusion to a similar extent. When the 60 s trajectories that do not experience transient confinement are separated into fast ($D \geq 10^{-10}$ cm^2/s) and slow ($D < 10^{-10}$ cm^2/s) classes, we find that only the slow category exhibits anomalous diffusion (Table 5), whereas the fast class undergoes Brownian motion.

Glycosphingolipids Undergo Confined Diffusion to a Significantly Greater Extent Than Phospholipids. Because there has been much speculation about the possible associations of GPI-anchored proteins with glycosphingolipid domains, we hypothesized that glycosphingolipid domains were causing the confinement of Thy-1 on C3H fibroblasts. We used SPT to follow the movements of these two types of lipids, GM1, a representative glycosphingolipid and putative component of GSL-enriched domains, and fl-PE, a phospholipid analog that had been incorporated into the plasma membrane. As shown in Table 2, we determined that 35% of GM1 exhibited confined diffusion to domains that were ~370 nm in diameter, in good agreement with the 37% confined diffusion observed for Thy-1. Additionally, there is good agreement with the domain diameters and

Table 4: Valency of the Colloidal Gold Probe[a]

	6.6 s Trajectories								
	fast		slow		confined		stationary		
	D[b]	%	D	%	D	%	D	%	n
multivalent	8.1 ± 0.7	29%	0.35 ± 0.05	24%	0.98 ± 0.18 322 ± 38 nm[c]	37%	0.060 ± 0.014	10%	295
paucivalent	7.9 ± 1.0	32%	0.44 ± 0.16	19%	1.7 ± 0.5 400 ± 60 nm	39%	0.048 ± 0.019	10%	59

	60 s Trajectories		
	domain diameter (nm)	confinement time (s)	n
multivalent	260 ± 21	6.9 ± 0.8	29
paucivalent	278 ± 66	10.0 ± 2.9	8

[a] "Paucivalent" data were acquired with gold that had been conjugated to *anti*-Thy-1:goat IgG (1:1.5 mol/mol) (see text). "Multivalent" data are the larger Thy-1 data set described in Tables 1−3. All values are reported as mean ± SEM. [b] D ($\times 10^{-10}$ cm^2/s). [c] Diameter calculated as described in Table 2.

Table 5: Anomalous Diffusion Exponents (α) for 6.6 s and 60 s Trajectories[a]

6.6 s Trajectories			
molecule	fast	slow	confined
Thy-1	1.04 ± 0.01	0.42 ± 0.01	0.58 ± 0.01
Thy-1 (GSL depleted)	1.03 ± 0.01	0.62 ± 0.01	0.47 ± 0.03
GM1	0.98 ± 0.01	0.71 ± 0.01	0.61 ± 0.01
fl-PE	0.95 ± 0.01	0.46 ± 0.01	0.35 ± 0.01

60 s Trajectories				
molecule	fast	n	slow	n
Thy-1	0.92 ± 0.01	20	0.41 ± 0.01	114
Thy-1 (GSL depleted)	0.92 ± 0.01	15	0.53 ± 0.01	49
GM1	0.98 ± 0.01	9	0.49 ± 0.01	64
fl-PE	0.91 ± 0.01	13	0.52 ± 0.01	37

[a] The anomalous diffusion exponent is calculated from the initial slope of $\alpha - 1$ from the averaged log ($<r^2>/\tau$) versus log τ plots for each transport class (see Figure 3B) (*48*). Trajectories of 60 s that do not exhibit transient confinement were classified into two categories based upon their diffusion coefficients. $D \geq 10^{-10}$ cm^2/s were classified as fast, and $D < 10^{-10}$ cm^2/s were classified as slow. The values are reported as the mean ± SEM.

confinement times between Thy-1 and GM1 that were determined from analyses of the 60 s trajectories (Table 3). As with Thy-1, GM1 also experiences anomalous diffusion in the slow and confined classes, with $\alpha \approx 0.6-0.7$ (Table 5).

For cells that had fl-PE incorporated immediately preceding a SPT experiment, we observed that the fast diffusing class of fl-PE had diffusion coefficients [$(5.6 \pm 0.6) \times 10^{-10}$ cm^2/s] comparable to GM1 and Thy-1 (see Table 1), but only 16% of the fl-PE exhibited confined diffusion to domains that averaged ∼230 nm in diameter (Table 2). The 6.6 s results for confinement were corroborated by results from the longer observations (Table 3). The slow and confined classes of fl-PE exhibit anomalous diffusion, similar to that observed for Thy-1 and GM1 (see Table 5).

Thy-1 Is Less Confined in Glycosphingolipid-Depleted Cells. To test the hypothesis that glycosphingolipid domains were confining the movements of Thy-1, we performed SPT experiments on cells that had been depleted of either glycosphingolipids or cholesterol to determine possible effects on the extent of confined diffusion of Thy-1. The glucosylceramide synthase inhibitor D-*threo*-1-phenyl-2-decanoylamino-3-morpholino-1-propanol (PDMP) (*32*−*34*) was added to the medium, and cells were incubated in the presence or absence of 10 μM PDMP for 4 days after plating cells onto coverslips. The glycosphingolipid expression was reduced (39 ± 5)% in the presence of this inhibitor. Qualitatively, this reduction in glycosphingolipid expression resulted in a marked reduction of fluorescence when GM1 was labeled with fluorescein-conjugated cholera toxin B on treated cells as compared to that of untreated cells (data not shown). The morphology of C3H cells in the presence of 10 μM PDMP for 4 days (Figure 6, top panel) was noticeably different from control cells (Figure 6, bottom panel) in that large spherical features were present in the perinuclear region in the treated cells and the lamellae were quite flat and featureless, similar to that observed in other studies using PDMP to lower GSL levels (*32*, *33*). We found that a smaller fraction of Thy-1 (28% versus 37% for the control cells) was confined to regions that are reduced in size ∼1.5-fold, as compared to Thy-1 confinement on untreated fibroblasts (Table 2). Longer observations confirmed that the domains confining Thy-1 decreased in size (from ∼260 to ∼165 nm) in the glycosphingolipid-depleted fibroblasts (Table 3). Thy-1 on the PDMP treated cells still underwent anomalous diffusion to a similar extent as Thy-1 on normal fibroblasts (Table 5).

Because the glycosphingolipid domains have been suggested to be enriched in cholesterol (*2*, *3*, *36*), we also depleted C3H cells of cholesterol. Again, cells were incubated for 4 days, in the presence or absence of LDL-depleted serum and the biosynthetic inhibitor mevastatin (*35*, *36*). The middle panel of Figure 6 shows the herniated cell edges and the vesicular features of the cell surface that were commonplace on cholesterol-depleted cells. We observed that the expression of Thy-1 on the surfaces of cholesterol-depleted cells was markedly reduced, as judged by immunofluorescence microscopy (data not shown), in agreement with the previous observations for the expression of the GPI-anchored proteins gD1-DAF (*51*) and CD14 antigen (*52*) on similarly depleted cells. Colloidal gold conjugated to *anti*-Thy-1 did not bind to the cholesterol-depleted cells at levels greater than background binding (<5 bound gold particles/cell) so that reliable SPT measurements were not possible. In addition, we were not able to carry out SPT experiments on GM1 of the cholesterol-depleted cells because the highly vesicular cell surface of these cells prohibits facile detection and analysis of the colloidal gold probes due to interference from the cellular structures appearing in the image.

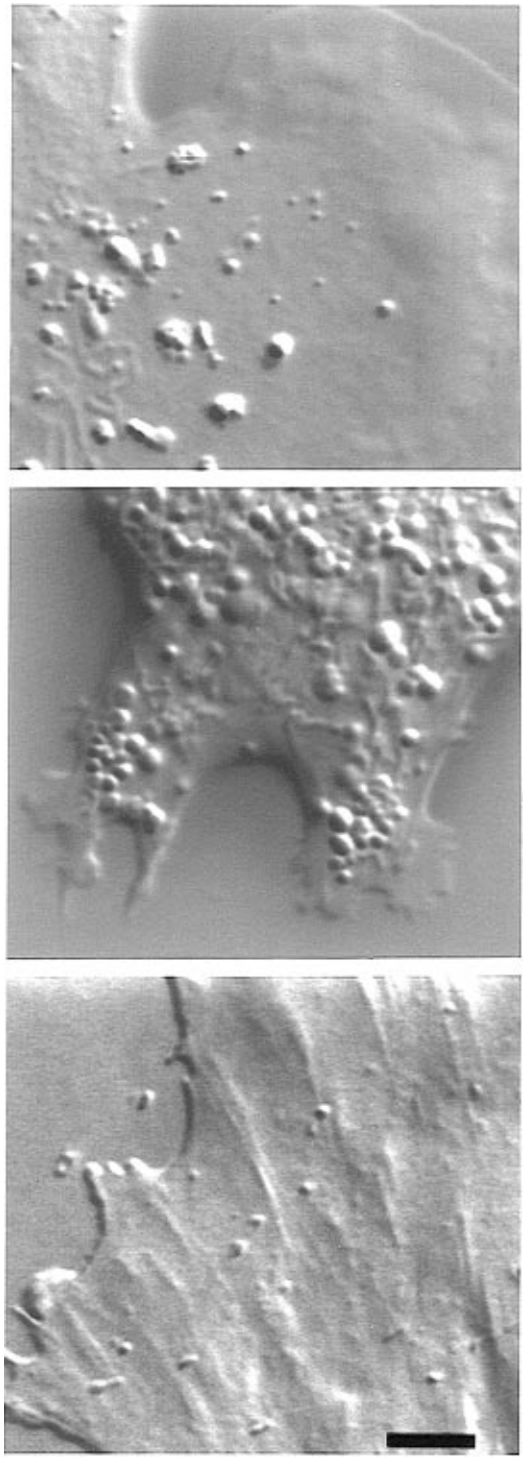

FIGURE 6: Lipid depleting medium changes the morphology of C3H fibroblasts. (Top) The lamella of cells that have been in the presence of glycosphingolipid depleting media for 4 days are quite flat and featureless, except for some large spherical structures in the perinuclear region. (Middle) Cells that are grown in the presence of cholesterol depleting media for 4 days are not well spread, are highly vesicular throughout the cells, and have herniated cell edges. (Bottom) The lamella of normal cells, 4 days after plating, are well spread and featureless. Bar, 4 μm.

The Fractions of Confined Diffusion Remain Similar While the Fractions of Slowly Diffusing Thy-1 and GM1 Decrease on Triton X-100-Extracted Cells. When cells are treated with low concentrations of Triton X-100 (TX-100), membrane proteins that are not bound to the cytoskeleton and phospholipids are removed, leaving behind residual membrane made up primarily of proteins bound to the cytoskeleton and GSL-enriched domains (*53*, *54*). We treated cells with 0.1% TX-100 to observe the effects of detergent extraction on the lateral mobilities of Thy-1 and GM1. After extraction with TX-100, large holes that were several micrometers in diameter within regions of continuous membrane were observed by fluorescence microscopy of Thy-1 and GM1 (data not shown), similar to that observed by Mayor and Maxfield (*54*). As shown in Table 6, the sizes of the confining domains as well as the fractions of confined diffusion for both molecules agree with the control cells (Table 2); however, the fractions of slowly diffusing Thy-1 and GM1 decreased 2-fold after TX-100 extraction. Interestingly, the stationary fractions of Thy-1 and GM1 roughly doubled after extraction with the detergent, as compared to unextracted control cells (compare Tables 2 and 6).

Table 6: Effect of TX-100 Extraction on Thy-1 and GM1 Mobility

	6.6 s Trajectories				
	fast	slow	confined	stationary	*n*
Thy-1	26%	13%	42% 280 ± 23 nm[a]	18%	76
GM1	40%	7%	31% 283 ± 28 nm	21%	70

[a] Diameter calculated as described in Table 2.

DISCUSSION

In this paper, we have described a method for classifying trajectories from short time SPT experiments into four modes of lateral transport, fast diffusion, slow diffusion, confined diffusion, and a stationary fraction that is unable to move significant distances during the experimental time scale. We have also applied the probability profile analysis to the longer SPT molecular trajectories to identify periods of transient confinement. We used these analyses to compare the lateral mobilities of Thy-1, GM1, and fl-PE, as shown in Tables 1−3. We find that a significant fraction of Thy-1 and GM1 (35−40%) is transiently confined for 7−9 s to lateral domains that are 260−370 nm in diameter. In contrast to these results, a reduced fraction of fl-PE (16%) is confined for ∼6 s to regions that are significantly smaller in size (∼225 nm), which might be due to interactions between the saturated acyl chains of fl-PE and the other domain components. Schroeder *et al.* (*55*) have suggested that these acyl chain interactions are critical for the observed detergent resistance of the glycolipid-enriched domains. Because we have agreement between three fundamentally different methods of estimating domain size (the probability profile analysis for the 60 s tracks and, for the 6.6 s trajectories, extrapolation from the mean squared displacement plots for confined diffusion and the more exact value calculated from R_g^2 which is a parameter that is derived from the trajectories themselves), the smaller domain size observed for fl-PE is actually due to smaller spatial regions rather than possibly being attributed to faster escape times of fl-PE from the confining regions.

Results from earlier SPT experiments of fl-PE on C3H fibroblasts yielded a slightly higher D ($\sim 1 \times 10^{-9}$ cm^2/s) and suggested that fl-PE undergoes unconfined diffusion (*27*). The previous work, however, did not analyze trajectories with $D < 4 \times 10^{-10}$ cm^2/s which would account for the higher D reported by Lee *et al.* (*27*). In addition, we believe that the

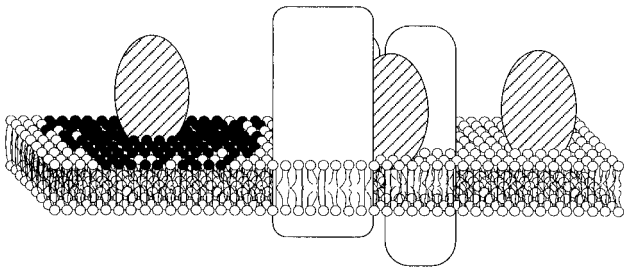

FIGURE 7: Model of molecular associations of Thy-1 in the plasma membrane that result in confined or slow diffusion. GPI-anchored proteins (hatched) are transiently associated with and confined by glycosphingolipid domains (black lipids). Slow, anomalous diffusion occurs when molecules encounter protein-rich regions (white proteins) in the plasma membrane. Fast Brownian motion occurs when molecules are located in relatively unobstructed regions of the membrane.

implementation of higher resolution centroid detection and a more sophisticated classification and analysis scheme contributed to the discrepancy with the earlier results.

By analyzing the lateral mobility of IgE receptors by FRAP and SPT, Feder *et al.* proposed recently that molecules undergo either Brownian motion or anomalous diffusion in the plane of the membrane (*50*). In their work, they classified SPT trajectories by individually derived α, such that those tracks with $\alpha \approx 1$ were categorized as Brownian motion, those with $0.1 < \alpha < 0.9$ were identified as anomalous diffusants, and those with $\alpha < 0.1$ were defined as immobile. As shown in Table 5, the values of our α [calculated from the averaged log ($<r^2>/\tau$) versus log τ plot for each transport category] correspond well with the categories of Webb and colleagues, with our fast diffusion undergoing Brownian motion and our stationary class equivalent to their immobile fraction (data not shown). Because we also classify trajectories based the shapes of the trajectories themselves (i.e., parameters describing the characteristic ellipses of gyration for individual trajectories) as well as the shapes of the mean squared displacement curves, we have identified two additional classes (slow and confined diffusion) which may correspond to the anomalously diffusing class observed by Webb and colleagues.

Our results suggest that confined diffusion may be attributed to glycosphingolipid-enriched domains in the plasma membrane (Figure 7). From a variety of biochemical analyses, the putative GSL domains have been proposed to be enriched in GPI-anchored proteins, lipid-anchored tyrosine kinases, glycosphingolipids, and cholesterol (*4*−*8*, *12*, *55*). The size of the confining domains for Thy-1 and GM1 (∼300 nm in diameter) is similar in size to the glycosphingolipid-enriched domains isolated by silica bead coating of endothelial cell surfaces (*9*) and the detergent insoluble membrane fractions sized by ultrafiltration (*56*). In addition, we find that the phospholipid analog fl-PE undergoes significantly less confined diffusion, and the sizes of the regions confining fl-PE (∼230 nm) are ∼1.5-fold smaller than those domains observed for Thy-1 and GM1 (∼300 nm), as shown in Tables 2 and 3. When the lateral mobility of Thy-1 was investigated on glycosphingolipid-depleted cells, we observed that the size of the confining domain and the fraction of Thy-1 experiencing transient confinement is reduced 1.5-fold as compared to the control cells. Moreover, detergent extraction leaves the confining regions essentially unchanged as judged from both their frequency and size. These results for transiently confined diffusion are consistent with preferential association of GPI-anchored proteins with glycosphingolipid domains (*1*−*7*, *10*, *12*). In the future, perhaps by simultaneously tracking fluorescent particles having different colors, it may be possible to demonstrate the colocalization of Thy-1 and GM1 to the same confining domains.

Edidin and colleagues suggested from results of photobleaching studies that the plasma membrane is composed of protein-rich and (relatively) protein-free domains (*17*, *57*). Our fast diffusion class is consistent with unobstructed Brownian motion within the protein−lipid continuum (Table 5). The anomalous, slow diffusion we observed may be attributed to diffusion through protein-rich domains, as depicted in Figure 7. When we used SPT to follow the movements of Thy-1 on cell surfaces after extraction with 0.1% TX-100 [leaving behind GPI-anchored proteins, glycosphingolipid-enriched domains, and membrane-spanning proteins bound to the cytoskeleton (*53*, *54*)], we observed that the fraction of slow diffusing molecules decreased ∼2-fold, suggesting that the detergent extractable fraction may provide some of the obstacles causing the slow anomalously diffusing class. In addition, the stationary fractions of Thy-1 and GM1 essentially doubled upon extraction with TX-100, which may correspond to the increase in clustering of GPI-anchored proteins observed under similar conditions with electron microscopy by Mayor and Maxfield (*54*).

In addition to protein−protein interactions controlling events such as signal transduction, recent work has suggested that local lateral heterogeneities in the plasma membrane may be important in regulation as well. The confining domains that we described in this paper could act to facilitate molecular interactions by increasing the local concentrations of specific molecules required for specialized functions (*19*), and work is beginning to emerge in support of this view. For example, glycosphingolipid domains have been implicated in initiating IgE receptor signaling on mast cells (*8*, *14*, *38*, *58*). In contrast, other work has shown that glycosphingolipid domains may exclude some proteins, such as the tyrosine phosphatase CD45, to inhibit the activity of nonreceptor kinases in T cell activation (*59*). Thus, it is essential to investigate the more subtle effects of the lateral organization of the plasma membrane in regulating and influencing functional molecular interactions.

ACKNOWLEDGMENT

We appreciate many fruitful discussions during the course of the project with Michael J. Saxton, Elizabeth de Beus, and Juliet Lee. Akira Ishihara graciously helped with computer program debugging.

REFERENCES

1. Brown, D. A. (1992) *Trends Cell Biol. 2*, 338−343.
2. Parton, R. G., and Simons, K. (1995) *Science 269*, 1398−1399.
3. Simons, K., and Ikonen, E. (1997) *Nature 387*, 569−572.
4. Brown, D. A., and Rose, J. K. (1992) *Cell 68*, 533−544.
5. Fra, A. M., Williamson, E., Simons, K., and Parton, R. G. (1994) *J. Biol. Chem. 269*, 30745−30748.
6. Olive, S., Dubois, C., Schachner, M., and Rougon, G. (1995) *J. Neurochem. 65*, 2307−2317.
7. Rodgers, W., Crise, B., and Rose, J. K. (1994) *Mol. Cell. Biol. 14*, 5384−5391.
8. Field, K. A., Holowka, D., and Baird, B. (1997) *J. Biol. Chem. 272*, 4276−4280.

9. Schnitzer, J. E., McIntosh, D. P., Dvorak, A. M., Liu, J., and Oh, P. (1995) *Science 269*, 1435−1439.
10. Deckert, M., Ticchioni, M., and Bernard, A. (1996) *J. Cell Biol. 133*, 791−799.
11. Robinson, P. J. (1991) *Immunol. Today 12*, 35−41.
12. Dráberová, L., Amoui, M., and Dráber, P. (1996) *Immunology 87*, 141−148.
13. Solomon, K. R., Rudd, C. E., and Finberg, R. W. (1996) *Proc. Natl. Acad. Sci. U.S.A. 93*, 6053−6058.
14. Thomas, J. L., Holowka, D., Baird, B., and Webb, W. W. (1994) *J. Cell Biol. 125*, 795−802.
15. Holowka, D., Hine, C., and Baird, B. (1996) *FASEB J. 10*, A1214.
16. Ishihara, A., Hou, Y., and Jacobson, K. (1987) *Proc. Natl. Acad. Sci. U.S.A. 84*, 1290−1293.
17. Edidin, M., and Stroynowski, I. (1991) *J. Cell Biol. 112*, 1143−1150.
18. Jacobson, K. A., Moore, S. E., Yang, B., Doherty, P., Gordon, G. W., and Walsh, F. S. (1997) *Biochim. Biophys. Acta*. (in press).
19. Sheets, E. D., Simson, R., and Jacobson, K. (1995) *Curr. Opin. Cell Biol. 7*, 707−714.
20. Edidin, M. (1993) *J. Cell Sci. Suppl. 17*, 165−169.
21. Jacobson, K., Sheets, E. D., and Simson, R. (1995) *Science 268*, 1441−1442.
22. Sheetz, M. P. (1993) *Annu. Rev. Biophys. Biomol. Struct. 22*, 417−431.
23. Kusumi, A., and Sako, Y. (1996) *Curr. Opin. Cell Biol. 8*, 566−574.
24. Saxton, M. J., and Jacobson, K. (1997) *Annu. Rev. Biophys. Biomol. Struct. 26*, 373−399.
25. Wilson, K. M., Morrison, I. E. G., Smith, P. R., Fernandez, N., and Cherry, R. J. (1996) *J. Cell Sci. 109*, 2101−2109.
26. Kusumi, A., Sako, Y., and Yamamoto, M. (1993) *Biophys. J. 65*, 2021−2040.
27. Lee, G. M., Zhang, F., Ishihara, A., McNeil, C. L., and Jacobson, K. A. (1993) *J. Cell Biol. 120*, 25−35.
28. Schmidt, C. E., Horwitz, A. F., Lauffenburger, D. A., and Sheetz, M. P. (1993) *J. Cell Biol. 123*, 977−991.
29. Ghosh, R. N., and Webb, W. W. (1994) *Biophys. J. 66*, 1301−1318.
30. Lee, G. M., Ishihara, A., and Jacobson, K. A. (1991) *Proc. Natl. Acad. Sci. U.S.A. 88*, 6274−6278.
31. Gelles, J., Schnapp, B. J., and Sheetz, M. P. (1988) *Nature 331*, 450−453.
32. Barbour, S., Edidin, M., Felding-Habermann, B., Taylor-Norton, J., Radin, N. S., and Fenderson, B. A. (1992) *J. Cell. Physiol. 150*, 610−619.
33. Radin, N. S., Shayman, J. A., and Inokuchi, J.-i. (1993) *Adv. Lipid Res. 26*, 183−213.
34. Vunnam, R. R., and Radin, N. S. (1980) *Chem. Phys. Lipids 26*, 265−278.
35. Goldstein, J. L., Basu, S. K., and Brown, M. S. (1983) *Methods Enzymol. 98*, 241−260.
36. Rothberg, K. G., Ying, Y.-S., Kamen, B. A., and Anderson, R. G. W. (1990) *J. Cell Biol. 111*, 2931−2938.
37. Schnaar, R. L. (1994) *Methods Enzymol. 230*, 348−370.
38. Chang, E.-Y., Zheng, Y., Holowka, D., and Baird, B. (1995) *Biochemistry 34*, 4376−4384.
39. Bartlett, G. R. (1959) *J. Biol. Chem. 234*, 466−468.
40. Fiske, C. H., and Subbarow, Y. (1925) *J. Biol. Chem. 66*, 375−400.
41. Gregson, N. A. (1993) in *Methods in Molecular Biology* (Graham, J. M., and Higgins, J. A., Eds.) pp 287−301, Humana Press, Totowa, NJ.
42. Jourdian, G. W., Dean, L., and Roseman, S. (1971) *J. Biol. Chem. 246*, 430−435.
43. Simson, R., Sheets, E. D., and Jacobson, K. (1995) *Biophys. J. 69*, 989−993.
44. Saxton, M. J. (1993) *Biophys. J. 64*, 1766−1780.
45. Sheets, E. D. (1997) Ph.D. Dissertation, 88 pp, University of North Carolina at Chapel Hill, Chapel Hill, NC.
46. Holifield, B. F., Ishihara, A., and Jacobson, K. (1990) *J. Cell Biol. 111*, 2499−2512.
47. Choquet, D., Felsenfeld, D. P., and Sheetz, M. P. (1997) *Cell 88*, 39−48.
48. Saxton, M. J. (1994) *Biophys. J. 66*, 394−401.
49. Saxton, M. J. (1996) *Biophys. J. 70*, 1250−1262.
50. Feder, T. J., Brust-Mascher, I., Slattery, J. P., Baird, B., and Webb, W. W. (1996) *Biophys. J. 70*, 2767−2773.
51. Hannan, L. A., and Edidin, M. (1996) *J. Cell Biol. 133*, 1265−1276.
52. Esfahani, M., Bigler, R. D., Alfieri, J. L., Lund-Katz, S., Baum, J. D., and Scerbo, L. (1993) *Biochim. Biophys. Acta 1149*, 217−223.
53. Fox, J. E. B., Reynolds, C. C., and Boyles, J. K. (1992) *Methods Enzymol. 215*, 42−58.
54. Mayor, S., and Maxfield, F. R. (1995) *Mol. Biol. Cell 6*, 929−944.
55. Schroeder, R., London, E., and Brown, D. (1994) *Proc. Natl. Acad. Sci. U.S.A. 91*, 12130−12134.
56. Cinek, T., and Horejsí, V. (1992) *J. Immunol. 149*, 2262−2270.
57. Yechiel, E., and Edidin, M. (1987) *J. Cell Biol. 105*, 755−760.
58. Pierini, L., Holowka, D., and Baird, B. (1996) *J. Cell Biol. 134*, 1427−1439.
59. Rodgers, W., and Rose, J. K. (1996) *J. Cell Biol. 135*, 1515−1523.

BI9710939